Component Swapping Modularity for Distributed Precision Contouring

Azad Ghaffari, *Member, IEEE,* and A. Galip Ulsoy, *Fellow, IEEE*

***Abstract*—Prior works use numerical simulations to verify component swapping modularity (CSM) for various systems. Moreover, current CSM algorithms do not investigate control parameter allocation for a realistic control configuration when the control consists of multiple parts. Thus, this work primarily focuses on presenting and experimentally validating an empirical methodology to allocate and calibrate various parts of the controller to improve CSM in a precision multi-axis servo-system. As a secondary contribution, the concept of a modified reference contour is introduced to simplify control allocation and to improve the modularity of the cross-coupling control (CCC) which is utilized to achieve high-precision contouring. First, the unified linear CCC algorithm is presented for multi-axis servo-systems. Initially, the sensitivity of the contouring algorithm versus the control parameters is studied numerically. Then, empirical calibration and sensitivity analysis are conducted to obtain the optimal set of control parameters. Hence, the lowest feasible contour error is obtained for possible configurations of the servo-system. It is shown that the results of the empirical analysis are consistent with those of the numerical analysis. Despite dramatic differences between the servo-system variants, experimental results show that full CSM is achieved with the same controller for the variants of the servo-system.**

***Index Terms*—Component swapping modularity, distributed control, precision contouring, cross-coupling control.**

I. Introduction

The simplest controller configuration is desirable to satisfy a given set of design criteria for all variants of a networked system composed of swappable components. Component swapping modularity (CSM) is a design measure to evaluate the flexibility of a modular control system to cope with the effect of variable system characteristics due to swapping a component with a comparable counterpart. A distributed control structure as shown in Fig. 1 has been proposed to improve CSM. The proposed structure includes a base and local controller. The base controller is the same for all variants of the system. The local controller, usually placed in the swappable component, is calibrated to achieve the best feasible closed-loop performance. Such component swapping modularity is achieved when desired performance, sufficiently close to a centralized controller optimized for each variant, is realized for the distributed controller structure in Fig. 1. Component swapping modularity is improved when a desired closed-loop performance is achieved with a low-order local controller. Various design algorithms to achieve CSM have been proposed, including the LMI-based Method [4], Direct Method [13], and 3-Step Method [1]. Numerical simulations have proven CSM design to be effective in various applications, including engine idle speed control [4], [11], variable camshaft timing engine [2], and battery swapping modularity in plug-in hybrid electric vehicles [12].

Authors are with Department of Mechanical Engineering, University of Michigan, Ann Arbor, MI 48109-2125, aghaffar@umich.edu and ulsoy@umich.edu.

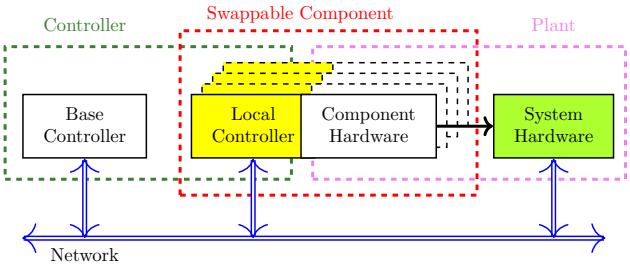

Fig. 1: Swappable smart component in a control network.

This work primarily focuses on developing an empirical methodology to allocate and calibrate control parameters in a realistic setting such that minimal control redesign is ensured when a component is swapped. Although conventional stability tools are used during the control design process, it should be noted that the contribution of this work is focused on experimental verification of CSM design in distributed precision contouring systems [7], [14]. The experimental setup includes a two-axis micro-precision servo-system with modular control boards and axes. The ultimate goal of a precision positioning application is to keep the actual contour identical to the reference contour. So, the notion of contour error is introduced which refers to the shortest distance from the current position to the reference contour.

The prevailing design trend for such contouring algorithms, known as variable-gain cross-coupling control (CCC), was originally introduced by Koren [9], [10] and is shown in Fig. 2. A basic CCC is comprised of two parts: 1) a contour error estimate (CEE) algorithm, composed of time-varying gains C_1 and C_2, which calculates the shortest distance from current position to the reference contour, and 2) an error compensator, $G_c(s)$, which is designed to drive the contour error to zero. The widely used CCC algorithms effectively improve contouring precision by compensating for the effect of uncertainty and by reducing contour error in multi-axis servo-systems.

The variable-gain CCC is a multi-input-multi-output compensator designed to incorporate coupling between all the axes. Therefore, due to the centralized nature of the variable-gain CCC, it is not feasible to fully distribute the parameters of the variable-gain CCC into local and base controllers [7], [14]. Thus, it is not possible to achieve full CSM for the variable-gain CCC. Ghaffari and Ulsoy [6] have introduced

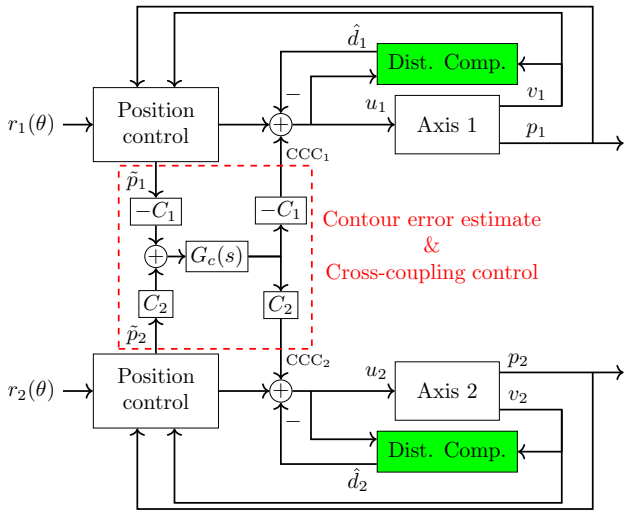

Fig. 2: Variable-gain CCC for a two-axis servo-system, originally proposed by Koren and Lo [9].

the modified error feedback concept to eliminate the need for a separate cross-coupling loop by modifying the error signal used in each of the position feedback loops. In this work, it is shown that the modified error feedback concept can be transformed into a modified reference contour concept such that the contouring algorithm is further simplified. In either case, the cross-coupling is achieved without changing the position control structure. The modified reference is a convex combination of the leading reference point and an estimate of the closest point of the reference contour to the current position which is obtained using the Newton-based CEE algorithm [6]. An optimal modified reference is obtained by properly tuning the positive gain $0 \leq \lambda < 1$, where λ remains the same for all the axes. So, $G_c(s)$, C_1, and C_2 are no longer needed which reduces the number of control parameters which in turn improves CSM.

The proposed contouring algorithm, shown in Fig. 3(b) for one axis, includes a position control, feedforward compensation, disturbance compensation, and the Newton-based CEE algorithm [6]. The modified reference contour reduces the compensator in the CCC algorithm to a proportional gain, λ, which further simplifies the tuning process of the control loop.

A servo-system is comprised of a power amplifier, electric machine, and linear stage. Swapping an axis, partially or entirely, with a compatible counterpart may change the system dynamics which may compromise the performance of the positioning or manufacturing process unless the modified system controller is re-calibrated. The proposed contouring algorithm is fully modular and suitable for use in CSM design. Therefore, it is convenient to conduct a sensitivity analysis of the control structure of each axis without considering the coupling effect from the other axis. Moreover, the result of the sensitivity analysis is used to optimally distribute the control elements between the local and base controllers such that the best contouring performance is achieved with the simplest local controller.

Given the proposed structure of the integrated controller (see Fig. 3(b)), first, a numerical sensitivity analysis is conducted to study the effect of each parameter on contouring performance. Then, an empirical methodology is developed to evaluate the sensitivity of the closed-loop performance with respect to the control parameters. It is shown that the empirical results are aligned with the numerical results. With careful design of the controller full CSM can be achieved even when all the control parts are located in the base controller. Thus, when an axis is swapped the control need not be re-calibrated to ensure the lowest feasible contour error.

The disturbance compensation dramatically attenuates the effect of friction and nonlinearity [3], [8]. An initial estimate of the axis dynamics is required to implement the disturbance compensation. So, the first step of the control design is to identify system dynamics of each axis to implement the disturbance compensation. Then, the compensated loop can be modeled using a more accurate linear model. Thus, the axis model after disturbance compensation is obtained to design the rest of the controller. Bode plots of the closed-loop system plus extensive experimental simulations show that the closed-loop system is robust with respect to the parameters of the disturbance compensation loop. So, a fixed set of reasonably large gains for the position control loop guarantees high-precision contouring. Thus, swapping modularity is improved.

The work of Ghaffari and Ulsoy [5] develops the empirical sensitivity analysis and provides the necessary steps for model identification and control design. This paper extends the results of Ghaffari and Ulsoy [5] in two directions: 1) a numerical sensitivity analysis is provided, and it is shown that the numerical results are in line with the experimental results. 2) After designing the CCC for CSM, extensive experiments are conducted to verify that the obtained controller indeed requires no tuning when one axis is swapped. Thus, demonstrating experimentally for the first time that full CSM is achieved.

The rest of the paper is organized as follows: Section II presents the integrated contouring algorithm using the modified reference concept. Section III explains the system configuration and the identification process. Section IV presents the numerical and empirical sensitivity analysis and provides experimental results and numerical analysis to support the obtained control parameter set. Section V concludes the paper.

II. Modified Reference and Integrated Contouring Algorithm

The dynamic equations of a single servo-axis can be represented as:

$$\frac{\mathrm{d}}{\mathrm{d}t}p = v \tag{1}$$

$$\frac{\mathrm{d}}{\mathrm{d}t}v = -bv + a\left(u + d\right), \tag{2}$$

where u is command, d is disturbance including load and friction, v is velocity, p is position, $k = a/b$ is the DC gain, and $\tau = 1/b$ is the time constant of the axis.

Assume the reference contour map is $r(\theta)$, where θ is a real number and indicates the current position along the reference path. Position and velocity error vectors of a multi-axis servo-system are defined as $\tilde{\boldsymbol{p}} = \boldsymbol{r}(\theta) - \boldsymbol{p}$ and $\tilde{\boldsymbol{v}} = \mathrm{d}\boldsymbol{r}(\theta)/\mathrm{d}t - \boldsymbol{v}$, where boldface letters indicate vectors, e.g.,

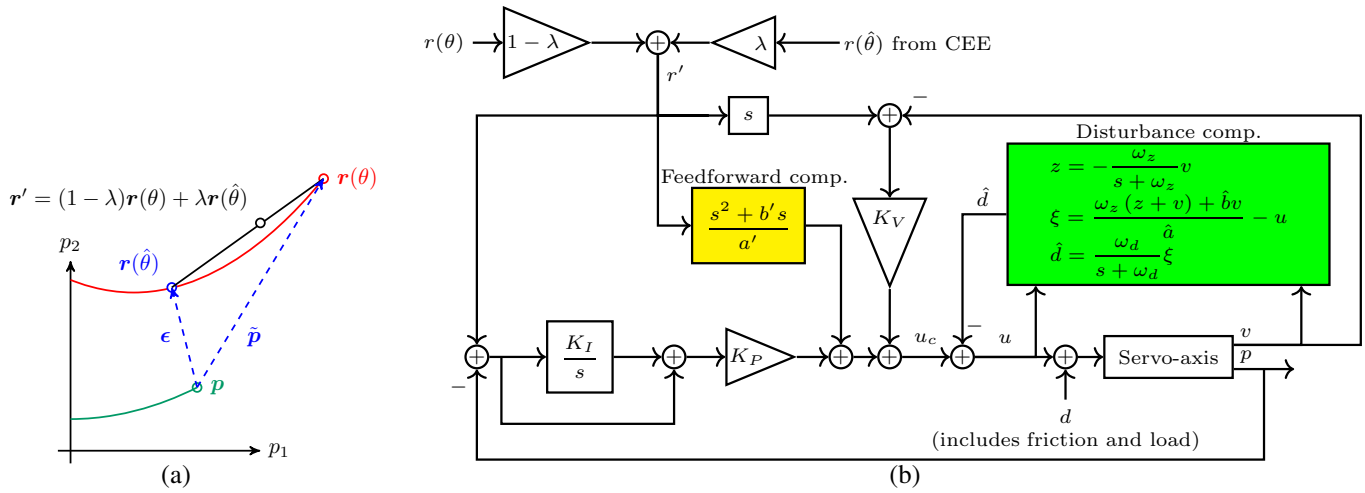

Fig. 3: (a) Modified reference improves contouring precision. (b) Integrated contouring control for one axis. Contour error estimate is calculated using the Newton method [6]. The reference contour, shown in (a) as $\boldsymbol{r}(\theta)$, is a vector and its projection along one axis is $r(\theta)$ as shown in (b).

$\boldsymbol{f} = [f_1\ f_2\ \cdots\ f_n]^T$ for a n-Axis system. The contour error, $\boldsymbol{\epsilon}^*$, is the shortest distance from the current position, $\boldsymbol{p}$, to the reference contour, $\boldsymbol{r}$. Let $\boldsymbol{\epsilon}^*$ occur at θ^*, i.e., $\boldsymbol{\epsilon}^* = \boldsymbol{r}(\theta^*) - \boldsymbol{p}$. Denote the contour error estimate as $\boldsymbol{\epsilon} = \boldsymbol{r}(\hat{\theta}) - \boldsymbol{p}$, where $\hat{\theta}$ is an estimate of θ^* which is obtained using the Newton-based CEE algorithm [6].

A. Modified Reference

Ghaffari and Ulsoy [6] have shown that the modified feedback concept facilitates CCC design by removing the contour error compensator from the control loop. Instead, the position control loop of each axis acts on the modified feedback along the relevant axis. Contouring precision is improved by properly tuning the ratio of the contour error and the position error in the modified error. Intuitively speaking, the modified error vectors determine in which direction the current point will progress which spans the area between $\tilde{\boldsymbol{p}}$ and $\boldsymbol{\epsilon}$. Please see Fig. 3(a). The modified error vectors are introduced as follows:

$$\begin{aligned} \check{\boldsymbol{p}} &= (1-\lambda)\,\tilde{\boldsymbol{p}} + \lambda\boldsymbol{\epsilon} \\ &= \boldsymbol{r}' - \boldsymbol{p} \end{aligned} \tag{3}$$

$$\begin{aligned} \check{\boldsymbol{v}} &= (1-\lambda)\,\tilde{\boldsymbol{v}} + \lambda\frac{\mathrm{d}}{\mathrm{d}t}\boldsymbol{\epsilon} \\ &= \frac{\mathrm{d}}{\mathrm{d}t}\boldsymbol{r}' - \boldsymbol{v}, \end{aligned} \tag{4}$$

where the modified reference contour is introduced as:

$$\boldsymbol{r}' = (1-\lambda)\,\boldsymbol{r}(\theta) + \lambda\boldsymbol{r}(\hat{\theta}), \qquad 0 \le \lambda < 1. \tag{5}$$

Without including the effect of contour error in the control loop, accurate position tracking is not feasible due to the wide range of reference contours, uncertainties, and external disturbances. The modified reference is another interpretation of the modified feedback concept which shows that one can directly include the effect of contour error in the modified reference instead of changing the feedback. As shown in Fig. 3(a), the modified reference redefines the leading point of the contour on a straight line between $\boldsymbol{r}(\theta)$ and $\boldsymbol{r}(\hat{\theta})$. Parameter λ is tuned such that desired contouring precision is achieved for a given set of reference contours. If $\lambda = 0$, there is no cross-coupling. Moreover, $\lambda = 1$ is not possible to achieve because controllability is lost between the current position and the reference point.

B. Integrated Control Algorithm

The experimental setup consists of linear stages driven by ball screw mechanisms. The ball screws exhibit considerable friction with stiction levels up to 10% of the command signal. So, it is desired to alleviate the effect of friction and external disturbance using the following disturbance estimator [3], [8]:

$$\frac{\mathrm{d}}{\mathrm{d}t}\hat{d} = -\omega_d\hat{d} + \omega_d\xi, \tag{6}$$

where

$$\xi = \frac{\omega_z\,(z+v) + \hat{b}v}{\hat{a}} - u, \tag{7}$$

$$\frac{\mathrm{d}}{\mathrm{d}t}z = -\omega_z z - \omega_z v, \tag{8}$$

where $\hat{a}$ and $\hat{b}$ are estimates of a and b, respectively. Also, ω_z and ω_d represent filter cut-off frequency for acceleration and disturbance estimators, respectively. An estimate of acceleration, $\dot{v}$, is obtained as $v + z$. Thus, ω_z should be large enough in comparison to b such that an accurate estimate of acceleration is obtained which is used to calculate ξ, which is an un-filtered estimate of the disturbance. So, to obtain a smooth estimate of disturbance, one can filter ξ using a first order low-pass filter with cut-off frequency ω_d. A reasonable ω_d falls between b and ω_z, i.e., $b \ll \omega_d \ll \omega_z$.

Denote $u = u_c - \hat{d}$. Then one can convert (2) to

$$\frac{\mathrm{d}v}{\mathrm{d}t} = -bv + a\left(u_c - \hat{d} + d\right). \tag{9}$$

Then, the transfer function of the compensated velocity loop, from u_c to v in Fig. 3(b), can be calculated using Laplace

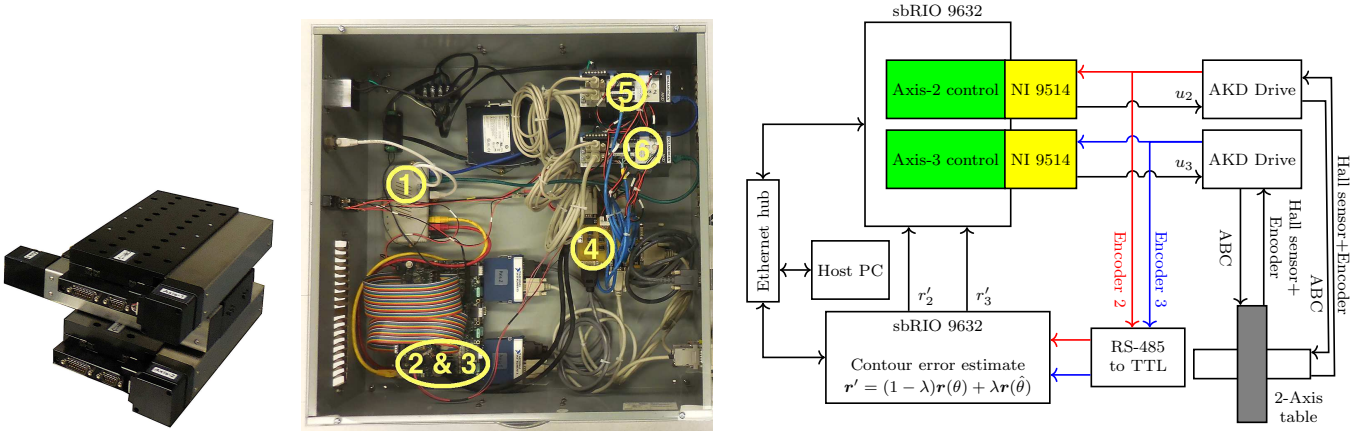

(a) (b) (c)

Fig. 4: (a) The servo-system is comprised of three linear axes, denoted Axis-2, Axis-3, and Axis-1, respectively from bottom to top. (b) Control box, including (1) Ethernet hub, (2 & 3) control boards, (4) interface circuit, and (5 & 6) servo-drives. (c) Schematic of the experimental setup. Axis-2 is swappable with Axis-1.

transformation of (6)–(9) and basic arithmetic operations which gives the following

$$V(s) = \frac{\mathcal{B}_u(s)}{\mathcal{A}(s)} U_c(s) + \frac{\mathcal{B}_d(s)}{\mathcal{A}(s)} D(s), \tag{10}$$

where

$$\mathcal{B}_u(s) = a\,(s+\omega_z)\,(s+\omega_d) \tag{11}$$

$$\mathcal{B}_d(s) = as\,(s+\omega_z) \tag{12}$$

$$\mathcal{A}(s) = s^3 + (\omega_z + b)\,s^2 + \left(\left(\omega_z + \hat{b}\right)\omega_d \frac{a}{\hat{a}} + \omega_z b\right) s + \\ + \omega_d \omega_z \hat{b} \frac{a}{\hat{a}}, \tag{13}$$

where $V(s), U_c(s)$, and $D(s)$ are Laplace transformations of $v(t), u_c(t)$, and $d(t)$, respectively.

From (10)–(13) one can observe that the steady state gain from the disturbance to velocity output is zero. Thus, the stiction level can be dramatically attenuated which enables the designer to fit a linear model to the compensated loop fairly precisely. In fact, the experiments show that after disturbance compensation one can fit a second order model to each axis with an accuracy above 95%. However, it should be noted that the DC gain from u_c to v equals $\hat{a}/\hat{b}$. Also, ω_z and ω_d are selected such that $b \ll \omega_d \ll \omega_z$. Thus, the location of the dominant pole is largely determined by $\hat{b}$. So, considering the physical limitations of the servo-axis, the designer can reshape the disturbance compensation loop to meet a desired transient performance. Moreover, care has to be taken that the upper level of disturbance attenuation, $\hat{a}/(\hat{b}\omega_d)$, stays as low as possible.

Since $b \ll \omega_d \ll \omega_z$, then it is reasonable to simplify (10) as a first order system free of disturbance. The resulting reduced model, which will be used to design the position control algorithm, is given as follows

$$G'(s) \;=\; \frac{P(s)}{U_c(s)} = \frac{a'}{s\,(s+b')}, \tag{14}$$

where a' and b' can be obtained using system identification. Using the following control law

$$u_c \;=\; K_V \check{v} + K_P \check{p} + \frac{K_P K_I}{s} \check{p} + \frac{s^2 + b's}{a'} r' \tag{15}$$

one can transform the position loop into

$$\frac{P(s)}{R'(s)} = \frac{a' K_P K_I}{s^3 + (b' + a' K_V)\,s^2 + a' K_P s + a' K_P K_I}, \tag{16}$$

where $R'(s)$ is the Laplace transformation of the modified reference along one of the axes $r' = (1-\lambda)r(\theta) + \lambda r(\hat{\theta})$. As shown in Fig. 3(a), instead of tracking the lead point of the reference contour, $\boldsymbol{r}(\theta)$, the proposed contouring control tracks the modified reference, $\boldsymbol{r}'$, which incorporates contour error in the tracking process. The shape and feedrate of the reference contour affect selection of λ. Also, when $\lambda = 0$ there is no cross-coupling between the axes of the servo-system.

III. System Configuration and Identification

The experimental setup and its schematic are shown in Fig. 4. Three linear stages are used to incorporate swapping modularity in the system. Axis-1 and Axis-2 are structurally identical with length and mass of 150 mm and 4.46 kg, respectively. Stage length of Axis-3 is 100 mm and stage mass is 3.67 kg. The rest of the electrical and mechanical technical characteristics are the same for the three axes and are listed in Table I. The CSM experiments are conducted on a servo-system composed of axes (2,3). Then, Axis-2 is swapped with Axis-1. Also, to highlight the differences caused by swapping Axis-2 with Axis-1, the three axes are installed in the following order, from bottom to top: Axis-2, Axis-3, and Axis-1. Please see Fig. 4(a). So, Axis-1 works as an external disturbance for axes (2,3) which causes considerable variation between dynamics of axes (1,3) and those of axes (2,3). The objective is to design an optimal contouring algorithm with the highest level of CSM for the given servo-system.

As explained in Section II, disturbance compensation plays a major role in improving closed-loop performance. Thus, the

Parameter	Value	Unit
Drive	Ground ball screw	–
Motor	Brushless servo 3-phase	–
Encoder	0.125 μm rotary	–
Encoder output	A quad B, index	–
Linear accuracy	12	μm
Linear Repeatability	2	μm
Max. linear velocity	150	mm/s
Screw lead	2	mm

TABLE I: System parameters for the linear stages.

steps to design the disturbance compensation are explained first. The disturbance estimate is given by (6)–(8). So, the values of $\hat{a}$ and $\hat{b}$, which are estimates of a and b, respectively, are required to implement the disturbance estimator.

Stiction is discontinuous and a major source of disturbance in ball screw mechanisms, consuming up to 10% of the control power signal. The stiction information for each axis is obtained experimentally and shown in Fig. 5(a). On average, the stiction consumes 5.5%, 8.8%, and 7.7% of the control signal for Axis-1, Axis-2, and Axis-3, respectively. Also, the friction level is slightly higher for Axis-2 because Axis-2 is installed under axes (3,1). Thus, linear models cannot fit the system dynamics precisely, unless the friction is compensated using a static or dynamic compensator. The dynamic disturbance compensation in Fig. 3(b) relies on the estimates of the system parameters a and b, and dramatically affects contouring performance. So, $\hat{a}$ and $\hat{b}$ are initialized using the result of an open-loop system identification. The results obtained are $\hat{a} \in \{1695, 648, 1116\}$ and $\hat{b} \in \{10.1, 6.5, 5.8\}$. As expected, the response time is 55% faster, and the DC gain is 70% larger for Axis-1 in comparison to those of Axis-2.

After disturbance compensation, one can fit a linear model to each axis with an accuracy of more than 95% and use the linear model to design the position control loop. So, a closed-loop system identification is conducted to obtain the dynamic model of each axis after disturbance compensation. A schematic of the closed-loop system identification is shown in Fig. 5(b). The exact model of the compensated velocity loop is given by (10). However, it is assumed that $b \ll \omega_d \ll \omega_z$. So, one can accurately replace (10) with a first-order system:

$$\frac{V(s)}{U_c(c)} = \frac{a'}{s+b'}. \tag{17}$$

The equivalent transfer function of Fig. 5(b) is

$$G_{\mathrm{id}}(s) \quad = \quad \frac{P(s)}{R(s)} = \frac{a'K_P}{s^2 + (b' + a'K_V)\, s + a'K_P}. \tag{18}$$

The controller gains are selected as $K_P = 4$ and $K_V = 0.1$. The identification results obtained are $a' = \{873, 754, 801\}$ and $b' = \{19.7, 24.7, 19.9\}$. The variation in the values of a' and b' is relatively small. As noted previously, except for mass and length, the three axes have the same physical characteristics. Thus, it can be concluded that the disturbance compensation effectively attenuates external disturbances and axis friction. So, the resulting linear models are relatively close.

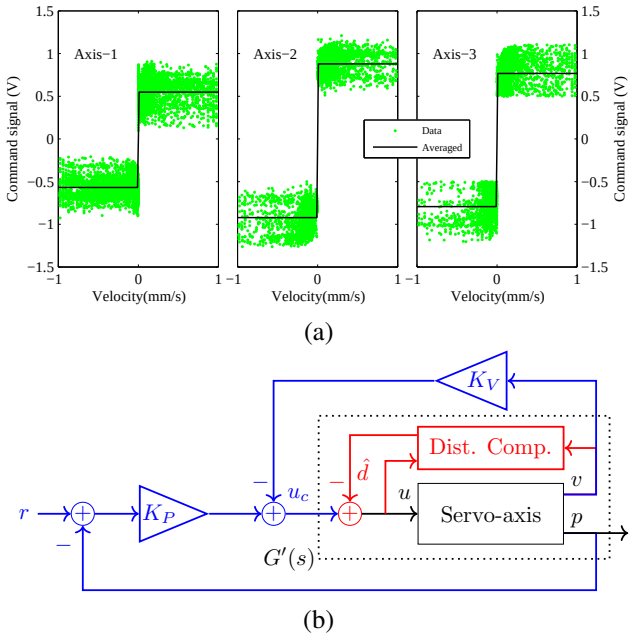

Fig. 5: (a) Stiction identification. (b) Closed-loop system identification with disturbance compensation.

IV. Control Sensitivity Analysis and Experimental Verification of Swapping Modularity

An overview of the control algorithm for one servo-axis is shown in Fig. 3(b). Tunable control parameters are selected as

$$\Omega = \left\{\hat{a}, \hat{b}, K_V, K_P, K_I, a', b'\right\}. \tag{19}$$

Assume a part of the multi-axis servo-system is swapped with a compatible counterpart. The worst case scenario is to achieve CSM by re-calibrating all the control parameters. The objective, however, is to reduce the contour error to its minimum feasible level by tuning the fewest number of control parameters. Apart from the modified reference loop which uses the CEE algorithm, each axis consists of four loops: 1) disturbance compensation, 2) velocity, 3) position, and 4) integral action. Sensitivity analysis is undertaken numerically and empirically to study the effect of each parameter on contouring precision. It is shown that the experimental results are aligned with the numerical results.

The disturbance compensation is initialized as explained in Section III. Then, the closed-loop identification is conducted to obtain the compensated model for each axis; the results of which are used to tune the rest of the control loops. The outermost loop is tuned based on the following reference model

$$\frac{P(s)}{R'(s)} = \frac{\alpha\omega_n^2}{(s^2 + 2\zeta\omega_n + \omega_n^2)\,(s+\alpha)}. \tag{20}$$

The control gains are calculated as

$$K_I \quad = \quad \frac{\alpha\omega_n}{2\alpha\zeta + \omega_n} \tag{21}$$

$$K_P \quad = \quad \frac{2\alpha\zeta\omega_n + \omega_n^2}{a'} \tag{22}$$

$$K_V \quad = \quad \frac{\alpha + 2\zeta\omega_n - b'}{a'} \tag{23}$$

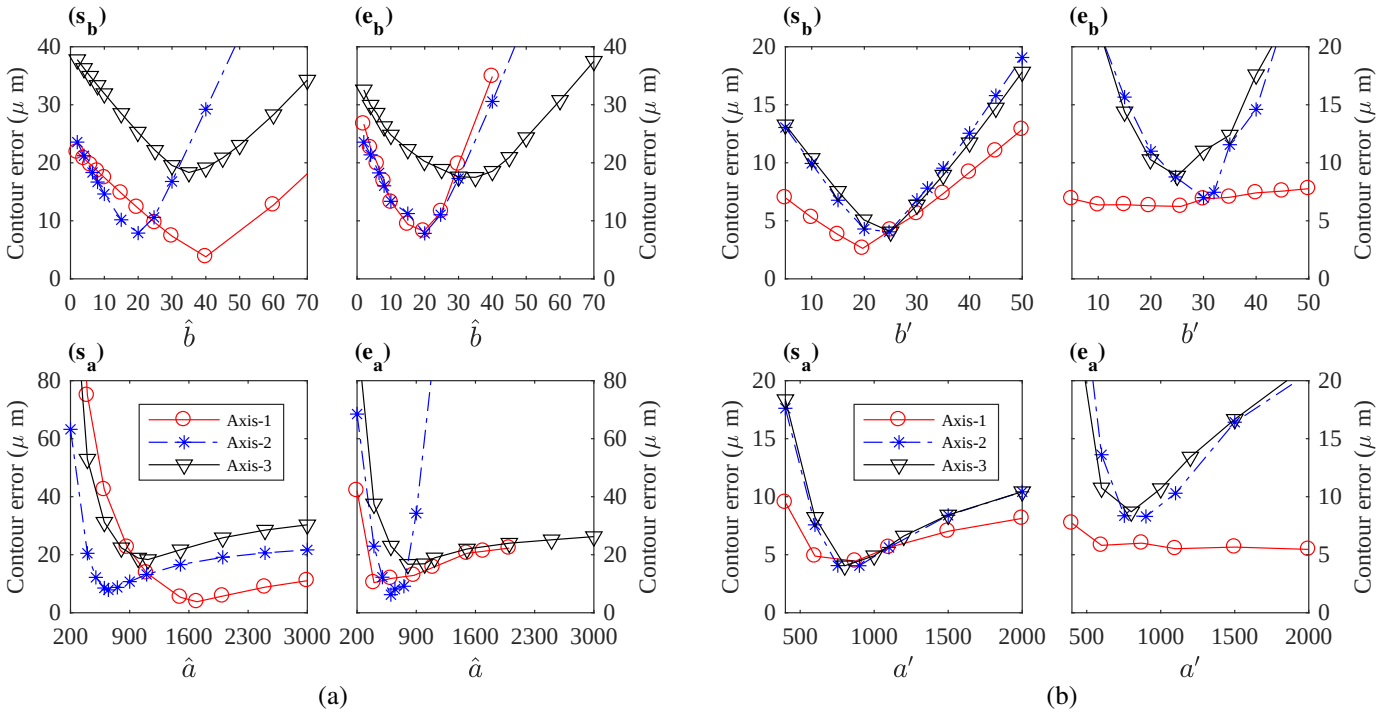

Fig. 6: Variation of contour error versus (a) disturbance compensation parameters, $\hat{a}$ and $\hat{b}$, and (b) feedforward compensation parameters, a' and b'. (s_b) and (s_a) simulations, and (e_b) and (e_a) experiments.

which show that the integral gain is independent of axis dynamic model. Table II lists the K_V, K_P, and K_I values for the desired $\omega_n = 25$ rad/s, $\zeta = 0.7$, and $\alpha = 35$ rad/s.

After initializing the contouring control, the cross-coupling is achieved with $\lambda = 0.75$. The control parameters are tuned sequentially, i.e., all parameters are fixed except one which is calibrated to achieve the smallest contouring error. The parameters are calibrated from innermost loop to the outermost loop in the following order: $\hat{b}_3, \hat{a}_3, \hat{b}_2, \hat{a}_2, K_{V3}, K_{P3}, K_{I3}, K_{V2}, K_{P2}, K_{I2}, b'_3, a'_3, b'_2$, and a'_2. When Axis-2 is swapped with Axis-1, the control parameters of Axis-1 are tuned in the following sequence: $\hat{b}_1, \hat{a}_1, K_{V1}, K_{P1}, K_{I1}, b'_1$, and a'_1. However, the control parameters of Axis-3 are not re-calibrated to highlight the level of CSM achieved only using the control parameters of the swapped axis. The results of the system identification are used to initialize the control parameters as listed in Table II.

The results of the numerical simulations and experiments are shown in Fig. 6(a)–(b) and 7. The numerical simulations closely follow the experimental results. Minor mismatches are because of modeling error. Contouring performance shows the lowest level of sensitivity to variation of control parameters of Axis-1. Also, except for the disturbance compensation parameters, the contouring precision shows similar sensitivity to the rest of the control parameters of Axis-2 and Axis-3.

Axis	$\hat{a}$	$\hat{b}$	K_V	K_P	K_I	a'	b'
1	1695	10.1	0.057	2.12	11.82	873	19.7
2	648	6.5	0.060	2.45	11.82	754	24.7
3	1116	5.8	0.062	2.31	11.82	801	19.9

TABLE II: Initial values of the control parameters obtained from model identification.

As Fig. 6 shows, the contouring precision has a local minimum versus variation in the parameters of the feedforward and disturbance compensators. Moreover, as Fig. 7 shows, the position control gains, if chosen large enough, have a negligible effect on contouring performance, the reason for which lies in the system configuration explained by (16). Assuming $K_V = 0.1, K_P = 4$, and $K_I = 11.8$, and incorporating 25% variation in $a' = 800$ and $b' = 20$, Fig. 8 shows that the variation in the closed-loop Bode plot is negligible which indicates low sensitivity of the closed-loop system with respect to large K_P and K_I. The sensitivity analysis of K_p and K_I, shown in Fig. 7, suggests an increase in K_P and K_I to make them as large as feasible. However, excessively large values of K_P and K_I push the dominant poles towards the imaginary axis and cause oscillations in contouring and consequent instability of the closed-loop system.

There are slight differences between sensitivity curves obtained from the simulations and experiments in Fig. 6(a) because of the effect of unknown nonlinear dynamics in the disturbance compensation loop. Nevertheless, Fig. 8 shows that the closed-loop system is relatively robust to the variations of the linear model of the disturbance compensation loop. Moreover, the system identification reveals that the disturbance compensation loop fits a second order linear model with accuracy more than 95%. Thus, one can overlook the differences between the results of the experiments and simulations in Fig. 6(a). Hence, the disturbance compensation parameters of Axis-1 and Axis-2 are selected identical.

The feedforward sensitivity analysis is shown in Fig. 6(b).

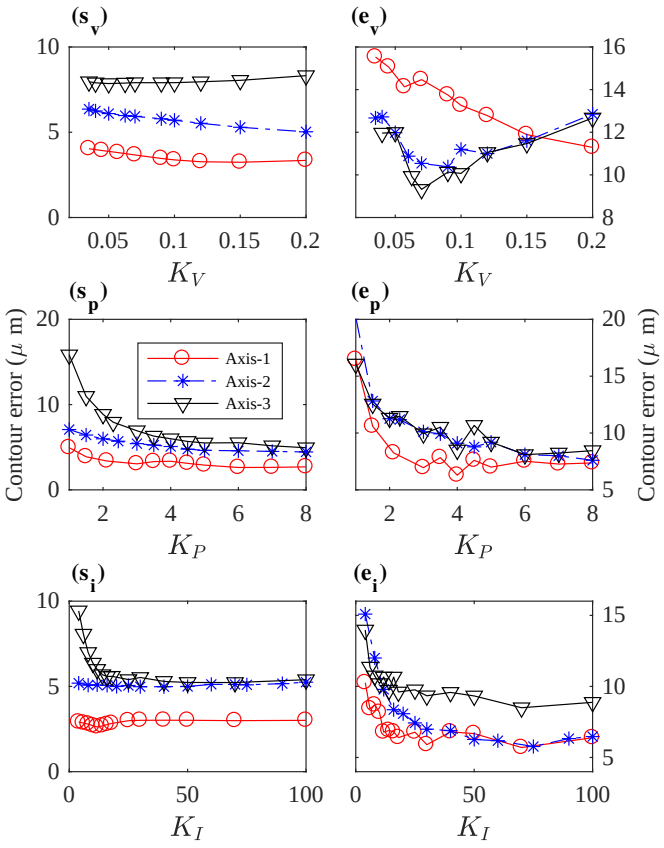

Fig. 7: Variation of contour error versus position control gains. (s_v), (s_p), and (s_i) simulations, and (e_v), (e_p) and (e_i) experiments.

The simulations and experimental sensitivity results are very close because the disturbance compensation efficiently alleviates the effect of uncertainties, friction, and external disturbances. The contour error shows the same level of sensitivity with respect to variation in b' and a' of Axis-2 and 3. The simulations suggest the same sensitivity curves for the feedforward parameters of Axis-1. Moreover, since the experiments show that the contour error only changes slightly when feedforward parameters of Axis-1 vary, then the feedforward parameters can be the same for all three axes. The result of the empirical sensitivity analysis is given in Table III.

Various experiments have been conducted, and it is concluded that swapping Axis-1 with Axis-2, or vice versa, does not affect the control parameters which indicates that full CSM is achieved without re-calibrating any of the control parameters. The experimental verification of CSM is shown in Fig. 9. The reference contour is a circle with radius 20 mm and frequency 0.5 Hz implemented as $r_1 = r_2 = 20\cos(\pi t)$ and $r_3 = 20\sin(\pi t)$. Because each axis changes direction two

Axis	$\hat{a}$	$\hat{b}$	K_V	K_P	K_I	a'	b'
1	600	20	0.1	4	11.8	900	30
2	600	20	0.1	4	11.8	900	30
3	1000	25	0.1	4	11.8	900	25

TABLE III: Control parameters obtained from the empirical sensitivity analysis.

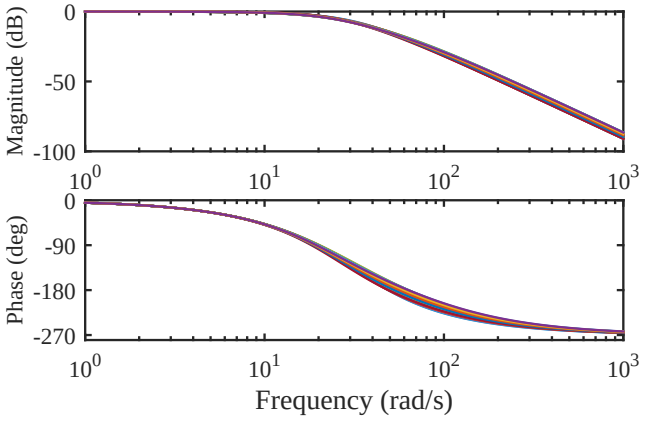

Fig. 8: Closed-loop Bode for 25% variation in $a' = 800$ and $b' = 20$.

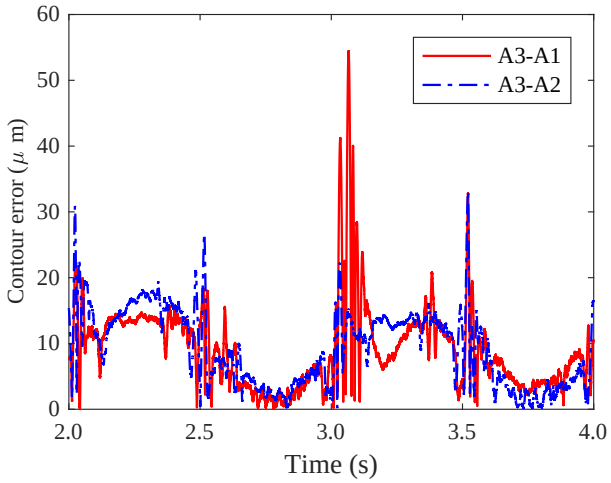

Fig. 9: Contouring performance when Axis-1 is swapped with Axis-2. Full CSM is achieved. The integral of contour error is 18.37 μm and 18.46 μm (i.e., nearly identical) for A3-A1 and A3-A2 configuration, respectively.

times during a full period, the friction then changes sign at the beginning of each quadrant which causes error spikes at times 2, 2.5, 3, and 3.5 s. The integral of contour error is 18.37 μm and 18.46 μm for A3-A1 and A3-A2 configuration, respectively. Hence, the obtained control parameters from the empirical analysis result in almost identical contouring performance with the same control for the axis combinations A3-A1 and A3-A2, which indicates full swapping modularity. Further experiments, not shown here, reveal that the obtained controls are indeed optimal and contouring is achieved with highest possible precision.

Achieving full CSM reduces time in tuning and calibration of control in distributed manufacturing systems. The conducted empirical analysis reveals that the linear model of the disturbance compensation loop provides an accurate basis for designing the proposed contouring algorithm. In other words, instead of designing the control loop using the original dynamics of the servo-system, one can use the results of the closed-loop system identification to guarantee near optimal contouring performance and full CSM. To achieve optimal

contouring, the empirical analysis can be conducted in a ball around the controller gains initialized using the results of the closed-loop system identification.

V. Conclusions

The unified contouring framework presented improves CSM in networked multi-axis servo-systems. The modified reference concept eliminates the need for a separate controller to ensure cross-coupling. Thus, the closed-loop system remains identical to the position control loop. So, the control can be designed using conventional methods. Flexible allocation and the modular structure of the modified reference contour improves CSM design and reduces tuning and calibration in distributed manufacturing systems. An empirical sensitivity analysis was conducted to optimally distribute the control parameters between the local and base controller. Extensive experiments were conducted, and the results showed that despite dramatic changes caused by swapping one of the axes, the highest level of CSM is achieved. In other words, it is experimentally shown for the first time that there exists an identical optimal configuration for the position control loop such that the lowest contour error is obtained for the available configurations of the two-axis servo-system. Moreover, the numerical simulation was proven to be fairly accurate. Thus, in future designs, one can opt out of the empirical analysis and conduct numerical sensitivity analysis to tune the control for CSM.

References

[1] M. Cakmakci and A. G. Ulsoy, "Improving component swapping modularity using bidirectional communication in networked control system," *IEEE/ASME Transactions on Mechatronics*, vol. 14, pp. 307–316, 2009.

[2] ——, "Swappable distributed MIMO controller for a VCT engine," *IEEE Transactions on Control Systems Technology*, vol. 19, pp. 1168–1177, 2011.

[3] W.-H. Chen, "Disturbance observer based control for nonlinear systems," *IEEE/ASME Transactions on Mechatronics*, vol. 9, pp. 706–710, 2004.

[4] A. Ghaffari and A. G. Ulsoy, "Design of distributed controllers for component swapping modularity using linear matrix inequalities," in *Proc. of IEEE International Conference on Advanced Intelligent Mechatronics*, 2016.

[5] ——, "Experimental verification of component swapping modularity for precision contouring," in *Proc. of American Control Conference*, 2017.

[6] ——, "Dynamic contour error estimation and feedback modification for high-precision contouring," *IEEE/ASME Transactions on Mechatronics*, vol. 21, pp. 1732–1741, 2016.

[7] C.-C. Hsieh, A.-P. Wang, and P.-L. Hsu, "CAN-based motion control design," in *Proc. of SICE Annual Conference*, 2003, pp. 3393–3398.

[8] M. Iwasaki, T. Shibata, and N. Matsui, "Disturbance-observer-based nonlinear friction compensation in table drive system," *IEEE/ASME Transactions on Mechatronics*, vol. 4, pp. 3–8, 1999.

[9] Y. Koren and C.-C. Lo, "Variable-gain cross-coupling controller for contouring," *CIRP Annals - Manufacturing Technology*, vol. 40, pp. 371–374, 1991.

[10] Y. Koren, "Cross-coupled biaxial computer control for manufacturing systems," *Journal of Dynamic Systems, Measurement, and Control*, vol. 102, pp. 265–272, 1980.

[11] S. Li, M. Cakmakci, I. V. Kolmanovsky, and A. G. Ulsoy, "Throttle actuator swapping modularity design for idle speed control," in *Proc. of American Control Conference*, 2009, pp. 2702–2707.

[12] S. Li, I. V. Kolmanovsky, and A. G. Ulsoy, "Distributed supervisory controller design for battery swapping modularity in plug-in hybrid electric vehicles," *ASME Journal of Dynamic Systems, Measurement and Control*, vol. 134, article no. 041013, 2012.

[13] ——, "Direct optimal design for component swapping modularity in control systems," *IEEE/ASME Transactions on Mechatronics*, vol. 18, pp. 297–306, 2013.

[14] Z. Wang, D. Yu, Y. Hu, and Y. Tao, "Design of distributed cross-coupled controller based on motion control bus," in *Proc. of Chinese Control and Decision Conference*, 2009, pp. 1662–1667.

Azad Ghaffari is a Postdoctoral Research Fellow in the Mechanical Engineering Department at the University of Michigan, Ann Arbor. He received the B.S. and M.S. degrees in electrical engineering from the K. N. Toosi University of Technology, Tehran, Iran, and the Ph.D. degree in mechanical and aerospace engineering from the Joint Doctoral Program between San Diego State University and the University of California, San Diego, CA, USA. His current research interests include distributed supervisory controller design for swapping modularity, cross-coupling control of multi-axis servo-systems, demand response in power systems, extremum seeking and its application to maximum power point tracking in photovoltaic and wind energy conversion systems, induction machines, power electronics, and sliding mode control.

A. Galip Ulsoy is C.D. Mote, Jr. Distinguished University Professor Emeritus of Mechanical Engineering and W.C. Ford Professor Emeritus of Manufacturing at University of Michigan, Ann Arbor. He received the Ph.D. from University of California at Berkeley (1979), M.S. from Cornell University (1975), and B.S. from Swarthmore College (1973). His research interests are in dynamics and control of mechanical systems. He has received numerous awards, including the 2008 Rufus T. Oldenburger Medal and the 2013 Charles Russ Richards Award from ASME, is a member of the National Academy of Engineering and is a Fellow of ASME, SME, IEEE and IFAC.